J Nanostruct 16(1): 1076-1090, Winter 2026

RESEARCH PAPER

Design, Characterization, and Use of Nano Fe_3O_4@Cellulose/Ti(IV) as an Efficient and Magnetically Recoverable Nano-Catalyst for the Synthesis of Highly Functionalized Tetrahydropyridines and DFT Calculations

Bi Bi Fatemah Mirjalil [1], Hadi Basharnavaz [1]*, Abdolhamid Bamoniri [2], and Sara Azad [1]*

[1] *Department of Chemistry, College of Science, Yazd University, Yazd, P.O.Box 89195-741, I.R.Iran*

[2] *Department of Organic Chemistry, Faculty of Chemistry, University of Kashan, Kashan, I.R.Iran*

ARTICLE INFO

Article History:
Received 12 September 2025
Accepted 20 December 2025
Published 01 January 2026

Keywords:
Highly functionalized tetrahydro pyridines
Magnetic catalyst
Nano-cellulose
Nano Fe_3O_4@cellulose/Ti(IV)
Supported Lewis acid

ABSTRACT

The facile two-step process for the preparation of nano Fe_3O_4@cellulose/Ti(IV) as a novel magnetic nano-solid acid catalyst is described, which includes the synthesis of nano Fe_3O_4@cellulose/Ti(IV) as a magnetic core-shell structure, followed by supporting titanium tetrachloride on the cellulosic shell. The structure, morphology, and magnetic properties of nano Fe_3O_4@cellulose/Ti(IV) were studied with some different techniques, such as Fourier transform infrared (FT-IR) spectroscopy, field emission scanning electron microscopy (FESEM), transmission electron microscopy (TEM), X-ray diffraction (XRD), X-ray fluorescence (XRF), vibrating sample magnetometry (VSM) and thermo-gravimetric analysis (TGA). The catalytic performance of this nano-catalyst has been studied in the synthesis of asymmetric highly functionalized tetrahydropyridines via a five-component condensation reaction of p-substituted anilines, aldehydes, and ethyl acetoacetate under thermal conditions. This procedure offers the advantages of mild reaction conditions, easy work-up, excellent yields, simple magnetic separation of the catalyst, and its recyclability for up to seven cycles without any considerable loss of efficiency, which is consistent with the results of DFT computation.

How to cite this article
Mirjalil B., Basharnavaz H., Bamoniri A., Azad S.. Design, Characterization, and Use of Nano Fe_3O_4@Cellulose/Ti(IV) as an Efficient and Magnetically Recoverable Nano-Catalyst for the Synthesis of Highly Functionalized Tetrahydropyridines and DFT Calculations. J Nanostruct, 2026; 16(1):1076-1090. DOI: 10.22052/JNS.2026.01.096

INTRODUCTION

In recent decades, magnetic nanoparticles (MNPs) have appeared as an excellent type of catalyst support because of their good stability, easy synthesis and functionalization, high surface area and facile separation by magnetic forces, as well as low toxicity and price [1,2]. Other important features of these magnetic catalysts are high catalytic activity, high degree of chemical stability in various organic and inorganic solvents, reusability, and benign character in the context of green chemistry. Among the various MNPs, magnetite (Fe_3O_4) is mostly used as a core magnetic support [3-5]. Fe_3O_4 nanoparticles have been prepared by precipitation [6], co-precipitation [7], and

* *Corresponding Author Email: fmirjalili@yazd.ac.ir*
h.basharnavaz@yazd.ac.ir

hydrothermal [8] methods. However, pure Fe_3O_4 nanoparticles are likely to form a large aggregation with fewer activating groups and are easily oxidized or dissolved in an acid medium [9]. To overcome these problems, Fe_3O_4 nanoparticles are coated with various materials such as surfactants [10], polymers [11,12], silica [13], and carbon [14] to form a core–shell structure. It is noteworthy that in many cases the protecting shells not only stabilize the nanoparticles but can also be used for further functionalization, for instance with other nanoparticles or various ligands, depending on the desired application [15].

Recently, polysaccharides as natural polymers have been used to prevent magnetite nanoparticles from aggregating, and represent an attractive choice for the preparation of functional materials [16-19]. Among polysaccharides, cellulose is one of the most abundant and renewable polymers in the world and has been widely studied in both academic and industrial research [20]. This biopolymer exhibits some excellent properties, including mechanical robustness, biodegradability, hydrophilicity, and biocompatibility [21]. Owing to these fascinating properties, cellulose has found a wide application in a variety of areas such as pharmacy, agriculture, medical science, industries and so many other related branches [22-27]. Specifically, the hydroxyl groups in cellulose provide active sites for numerous attractive chemical modifications. Thus, Cellulose can be used as an efficient support for bonding several functional groups to produce impressive biopolymer-based catalysts [28,29].

Within the family of cellulose derivatives, the nano-structure of the cellulose is a particularly appealing duo to combining important properties of cellulose with amazing features of nano-scale materials. Hence, one of the main goals of the present work is the preparation of nano-cellulose (NCs) by sulfuric acid hydrolysis of cotton and using it for the synthesis of nano Fe_3O_4@cellulose/Ti(IV) (Fe_3O_4@NCs/Ti(IV)) as a new, biodegradable, effective and reusable magnetic nano-catalyst.

Tetrahydropyridines (THPs) and their derivatives have potent pharmaceutical properties as antiemetic and antipsychotic agents [30,31], anticancer [32] and antimalarial [33]. THPs have been used as drugs in the treatment of diseases such as Alzheimer (GTS-21) [34] and central nervous system (CNS) disorders (RO-10-5824) [35-37]. Alkyl-1-aryl-4-(arylamino)-2, 6-di-aryl-1, 2, 5, 6-tetrahydro-pyridine-3-carboxylates are some important densely substituted tetrahydro pyridines. These compounds are synthesized via one-pot reaction of *p*-substituted anilines, *p*-substituted aldehydes, and alkyl acetoacetate. Recently, these compounds have been synthesized in the presence of catalysts such as $InCl_3$ [37,38], BDMS [39], L-proline/TFA [33], TBATB [40], I_2 [41], CAN [42], $ZrOCl_2 \cdot \mathbf{8H}_2O$ [43], $ZrCl_4$ [32], *p*-TsOH·H_2O [44], $Fe(NO_3)_3 \cdot \mathbf{9H}_2O$ [45], $FeCl_3/SiO_2$ [46], amberlite IRA400-Cl resin/I_2/KI [47], HOAc [48], $BF_3.SiO_2$ [49], nano-silica sulfuric acid [50], and $NiFe_2O_4$@SiO_2 [51]. Some of these catalysts suffer from drawbacks such as long reaction times and low yield. Therefore, the development of new solid acid catalysts with numerous advantages such as cost-effectiveness, environmentally benign, easy workup, and good stability for the synthesis of highly functionalized tetrahydropyridines is of prime importance.

Herein we wish to report nano Fe_3O_4@cellulose/Ti(IV) as a bio-based, magnetic, and effective heterogeneous nano-catalyst for the synthesis of Alkyl-1-aryl-4-(arylamino)-2, 6-di-aryl-1, 2, 5, 6-tetrahydro- pyridine-3-carboxylates via multi-component reaction of *p*-substituted anilines, *p*-substituted aldehydes and ethyl acetoacetate.

MATERIALS AND METHODS

General

All compounds were purchased from Merck, Aldrich, and Fluka chemical companies and used without additional purification. A refrigerated centrifuge (Appendorf Centrifuge 5417R) was used to prepare nano-cellulose. FT-IR spectra were run on a Bruker, Equinox 55 spectrometer. A Bruker (DRX-400 Avance) NMR was used to record the ^{1}H-NMR and ^{13}C-NMR spectra. Melting points were determined by a Buchi melting point B-540 B.V.CHI apparatus and were uncorrected. The X-ray diffraction (XRD) pattern was obtained by a Philips Xpert MPD diffractometer equipped with a Cu Ka anode (k=1.54 A°) in the 2θ range from 10 to 80°. Field Emission Scanning Electron Microscopy (FESEM) was obtained on a Mira 3-XMU. Transmission electron microscopy (TEM) was obtained using a Philips CM120 with a LaB6 cathode and an accelerating voltage of 120 kV. XRF analysis was done with Bruker, S4 Explorer instrument. The VSM measurements were performed using a vibrating sample magnetometer (Meghnatis Daghigh Kavir Co. Kashan Kavir, Iran).

Preparation of nano-cellulose from cotton

Cotton fibers were washed with distilled water several times and dried in an air-circulated oven at 100±2 °C until constant weight. Then they were chopped to an approximate length of 5-10 mm. The fibers were then treated with a 17.5 w/v NaOH solution at 100 ˚C for 12 hours under mechanical stirring. This treatment allowed purifying cellulose by removing other constituents like lignin, hemicellulose, wax, organic acids, and so on present in the fibers. Subsequently, fibers were filtered and washed with distilled water until the alkali was completely eliminated. It was then bleached with 100 ml of 1:1 aqueous dilution of 3.5% w/v sodium hypochlorite at 80 °C for 3 hours under mechanical stirring. The resulting alpha-cellulose was hydrolyzed partially using a 65% sulfuric acid aqueous solution with a cotton-to-acid weight ratio of 1–10 at 45 °C. After 1 hour, the obtained suspension was diluted with water five-fold to stop the hydrolysis reaction. The suspension was centrifuged at 12,000 rpm to separate the nano-cellulose from the acid solution. The washing with water and centrifuging was repeated four to five times to remove any remaining free acid.

Preparation of Fe_3O_4@NCs

1 g of nano-cellulose is dissolved in 100 mL of 0.05 M acetic acid solution; to which $FeCl_3 \cdot 6H_2O$ (3.51 g, 0.013 mol) and $FeCl_2 \cdot 4H_2O$ (1.29 g, 0.0065 mol) are added. The resulting solution is mechanically stirred for 4 h at 80 °C. Consequently, 6 mL of 25% NH_4OH is injected drop wise into the reaction mixture with constant stirring. After 30 min, the mixture is cooled to room temperature, and nano-cellulose coated over magnetic nanoparticles is separated by an external magnet, first washed with distilled water, then ethanol, and finally dried under vacuum at room temperature.

Preparation of nano Fe_3O_4@cellulose/Ti(IV)

In a well-ventilated system, $TiCl_4$ (5 mL) was added drop wise to the mixture of Fe_3O_4@NCs (5 g) in chloroform (20 mL). The mixture was stirred for one hour at room temperature. The resulting suspension was filtered, washed with chloroform, and dried at room temperature.

General procedure for synthesis of THPs

To a stirring solution of para-substituted anilines (2 mmol), ethyl acetoacetate (1 mmol), and nano Fe_3O_4@cellulose/Ti(IV) (0.03 g) in 5 mL EtOH, para-substituted benzaldehydes (2 mmol) was added, and the reaction mixture was refluxed for an appropriate time as indicated in Table 4. After completion of the reaction (monitored by TLC), the catalyst was separated by using an external magnet, and the reaction mixture

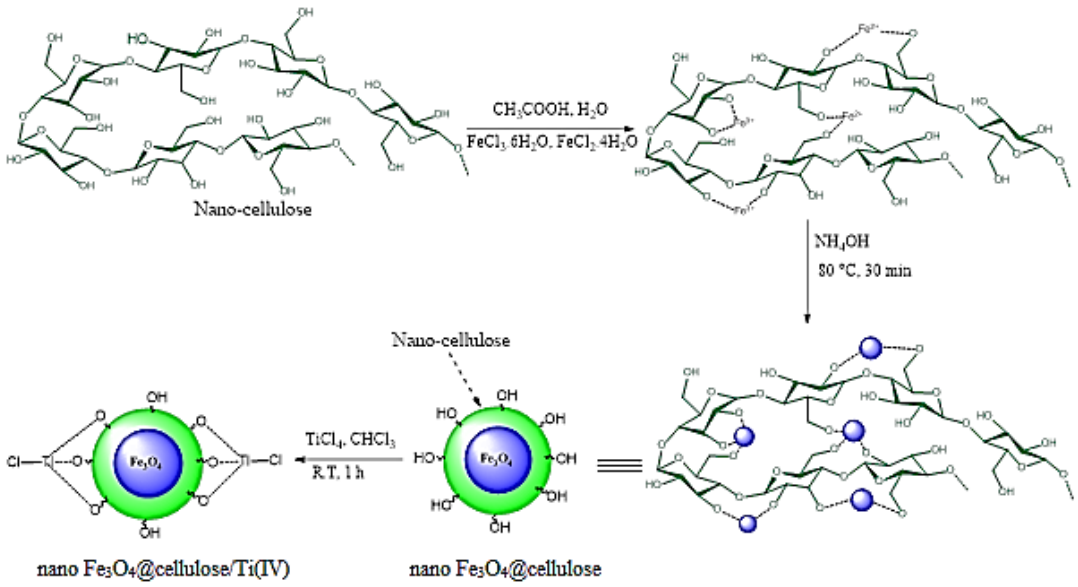

Fig. 1. Preparation of Nano Fe_3O_4@cellulose/Ti(IV)

was decanted. Subsequently, by adding water to the decanted solution, the product appeared as a pure solid in high yields. The recovered catalyst was washed 3 times with ethanol, dried, and reused for subsequent runs under the same reaction conditions.

RESULT AND DISCUSSION

Nano Fe_3O_4@cellulose/Ti(IV) was generally prepared in a two-step process. First, we synthesized Fe_3O_4@NCs by co-precipitation of Fe^{3+} and Fe^{2+} ions in the presence of nano-cellulose, and then we used it as magnetic support for bonding $TiCl_4$ (Fig. 1).

The magnetically heterogeneous catalyst, nano Fe_3O_4@cellulose/Ti(IV), is characterized by Fourier transform infrared (FT-IR) spectroscopy, FESEM, TEM, XRD, X-ray fluorescence (XRF), vibrating sample magnetometer (VSM), and thermo gravimetric analysis (TGA).

The FT-IR spectra of (a) nano-cellulose, (b) Fe_3O_4@NCs, and (c) nano Fe_3O_4@cellulose/ Ti(IV) are shown in Fig. 2. The FT-IR spectrum of nano-cellulose shows a broad band at 3337 cm^{-1} which corresponds to the stretching vibrations of OH groups. The absorption bands around 1055 and 1108 cm^{-1} display the stretching vibrations of the C-O bonds. For Fe_3O_4@NCs, cellulose absorptions appear in addition to the stretching vibrations of Fe-O groups at 586 and 634 cm^{-1}; indicating that the magnetic Fe_3O_4 NPs are coated by nano-cellulose. The FT-IR spectrum of nano Fe_3O_4@cellulose/Ti(IV) shows a characteristic peak at 794 cm^{-1} corresponding to C-O-Ti stretching according to the IR spectrum of $Ti(OBu)_4$ [52,53]. The peak at 406 cm^{-1} corresponds to the O-Ti-O bending vibrations [54]. The stretching vibrations of O–H bonds are observed at 3376 cm^{-1}. The 1585 cm^{-1} band might be due to the H-O-H bending vibration of adsorbed water [55]. In comparison with Fe_3O_4@NCs, bonding Ti to the cellulosic shell shifts Fe-O stretching vibrations to lower wavenumber (from 586 and 634 cm^{-1} to 558 and 606 cm^{-1}, respectively).

The particle size of nano-cellulose and nano Fe_3O_4@cellulose/Ti(IV) were investigated by field emission scanning electron microscopy (FESEM) and TEM in which the dimensions of them were achieved below 50 nm (Fig. 3).

The structure and phase purity of Fe_3O_4, Fe_3O_4@NCs, and nano Fe_3O_4@cellulose/Ti(IV) are studied using high angle XRD (Fig. 4). The bare Fe_3O_4 shows diffraction peaks at 2θ=30.4358°, 35.8507°, 43.4470°, 53.9461°, 57.4597°, and 63.0368° with FWHM equal to 0.4723, 0.4723, 0.4723, 0.7872, 0.6298, and 0.6298 respectively, which are quite

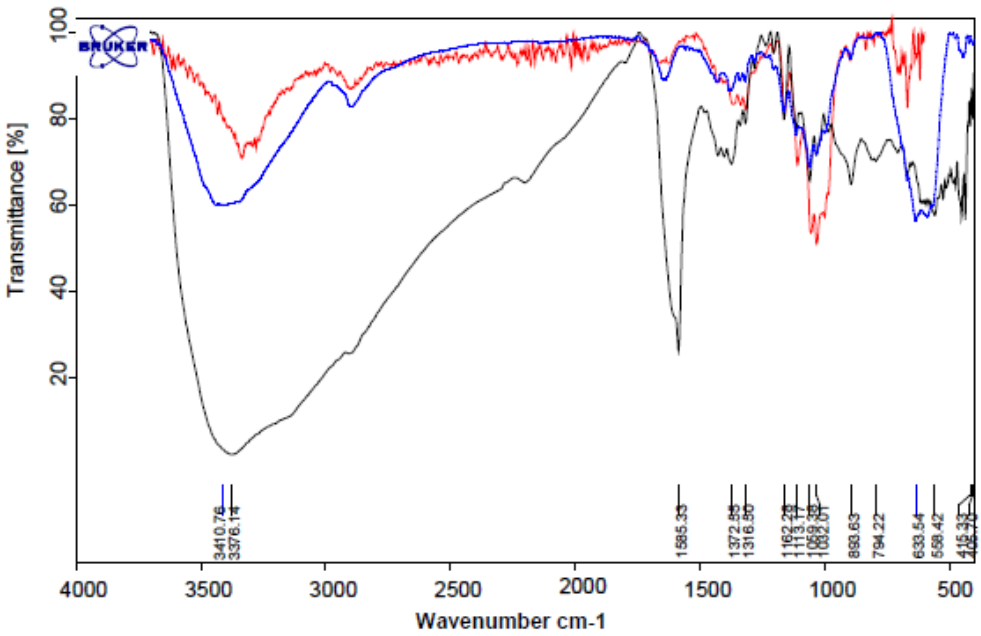

Fig. 2. FT-IR spectra of (a) nano-cellulose, (b) Fe_3O_4@NCs, and (c) Nano Fe_3O_4@cellulose/Ti(IV).

matched with the cubic spinel structure of pure Fe_3O_4 described in the literature (Fig. 4a) [56]. The same peaks were also observed in the Fe_3O_4@NCs XRD pattern, indicating retention of the crystalline spinel ferrite core structure during the cellulose-coating process. Moreover, a diffraction peak at 2θ =23.0444 appeared in the Fe_3O_4@NCs MNPs, which could be related to the cellulose coating of Fe_3O_4 NPs (Fig. 4b). The XRD pattern of nano Fe_3O_4@cellulose/Ti(IV) shows an amorphous

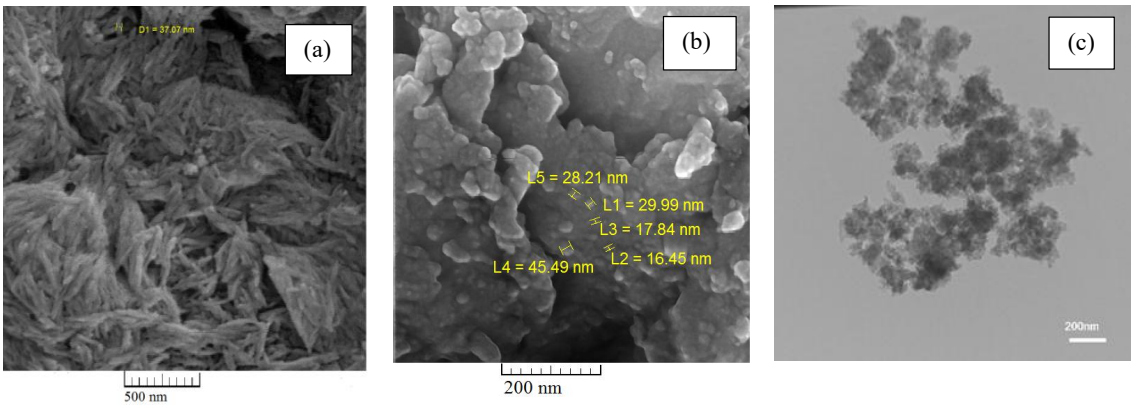

Fig. 3. (a) FESEM image of nano-cellulose, (b) FESEM of Fe_3O_4@NCs/TiCl, and (c) TEM of Nano Fe_3O_4@cellulose/Ti(IV).

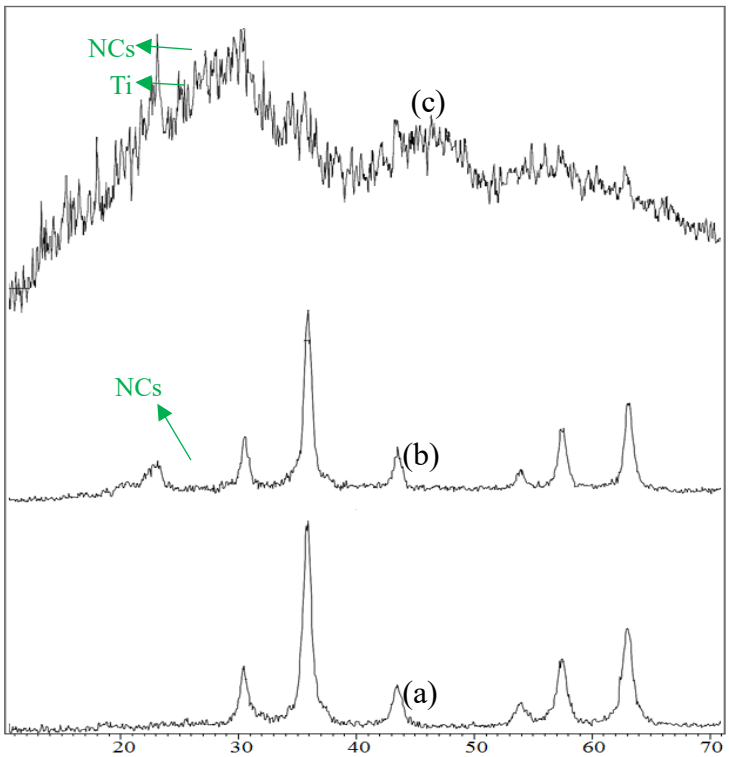

Fig. 4. XRD patterns of the (a) Fe_3O_4, (b) Fe_3O_4@NCs, and (c) Nano Fe_3O_4@cellulose/Ti(IV).

structure (Fig. 4c). The weak diffraction peaks at 2θ=29.9870°, 35.6108°, 46.5512°, and 56.0212° correspond to Fe_3O_4 cores (Fig. 4c). Other peaks at around 2θ=21°-23° reveal the existence of cellulose and bonding of Ti to cellulosic shell.

The chemical composition of the catalyst has been measured using XRF analysis (Table 1, Fig. 5). In order to obtain the Ti:Cl ratio in nano Fe_3O_4@ cellulose/Ti(IV) by XRF analysis, Killo Counts Per Seconds (KCPS) values of elements in the catalyst were compared with KCPS values of the same elements in pure samples, NaCl and TiO_2. By this comparison, the amount of Ti and Cl were obtained 4.51 g (0.1 mol) and 5.1 g (0.14 mol), respectively. Thus, the ratio of Ti:Cl in the catalyst is approximately 1:1.

To investigate the magnetic property of the catalyst, magnetic measurements were carried out using a vibrating sample magnetometer (VSM) in an applied magnetic field at 300 K. As shown in Fig. 6, no hysteresis loop and no remanence was detected, and also the coercivity value is zero for all samples, suggesting typical super paramagnetic property at room temperature. The saturation magnetization (Ms) values of Fe_3O_4, Fe_3O_4@NCs, and nano Fe_3O_4@cellulose/ Ti(IV) are 49.177, 33.057, and 6.062 emu/g, respectively. These results indicate that the magnetization of Fe_3O_4 decreased considerably by coating it with nano-cellulose and bonding $TiCl_4$ to OH groups of nano-cellulose. Even with this reduction in the saturation magnetization, the catalyst can still be efficiently

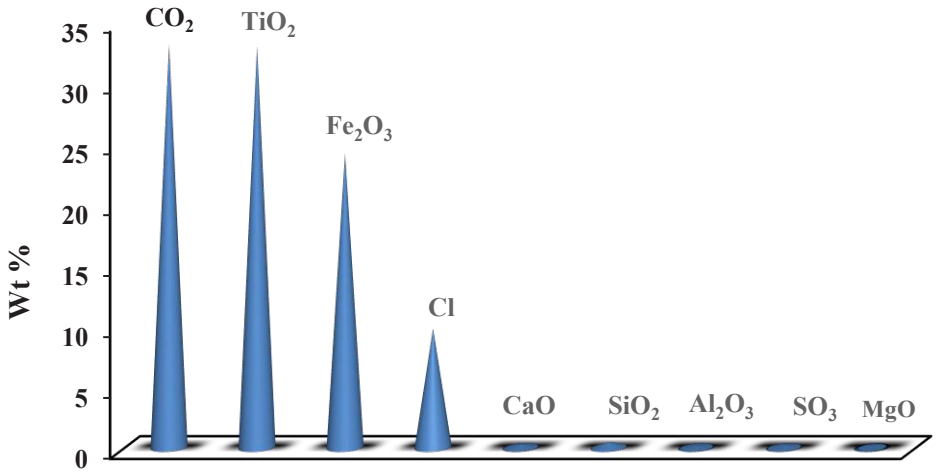

Fig. 5. XRF analysis of Nano Fe_3O_4@cellulose/Ti(IV).

Table 1. Results of XRF analysis of catalyst and pure samples NaCl and TiO_2.

elemental component	Nano Fe_3O_4@cellulose/Ti(IV)		NaCl		TiO_2	
	KCPS	wt %	KCPS	wt %	KCPS	wt %
Cl	44.6	9.75	516.5	62.4	-	-
TiO_2	174.3	32.9	-	-	2318.4	99.1
Fe_2O_3	164.3	24.1	-	-	-	-
CO_2	0.3	33	-	-	-	-
CaO	1.2	0.25	-	-	-	-
SiO_2	0.6	0.47	-	-	-	-
Al_2O_3	0.2	0.16	-	-	-	-
SO_3	0.5	0.186	-	-	-	-
MgO	0.1	0.07	-	-	-	-
Total	-	100.8	-	-	-	-

separated from the solution with a permanent magnet (as shown in the inset of Figure 5).

The thermal stability of nano Fe_3O_4@cellulose/Ti(IV) was investigated by TGA in the temperature range of 50-372 °C (Fig. 7). The TGA curve illustrates four mass-loss steps. Firstly, a very small weight loss (2.14%) from 50 to 100 °C is corresponded to the remove of catalyst moisture. Subsequently, there are two weight loss steps in the temperature ranges 100-135 and 150-180 °C (12.62 and 7.72%, respectively). Finally, the main weight loss (17.35 %), observed in the range of 180-372 °C, is attributed to the decomposition of cellulose units through the formation of levoglucosan and other volatile compounds [57]. The char yield of the catalyst at 372 °C is 58.62%.

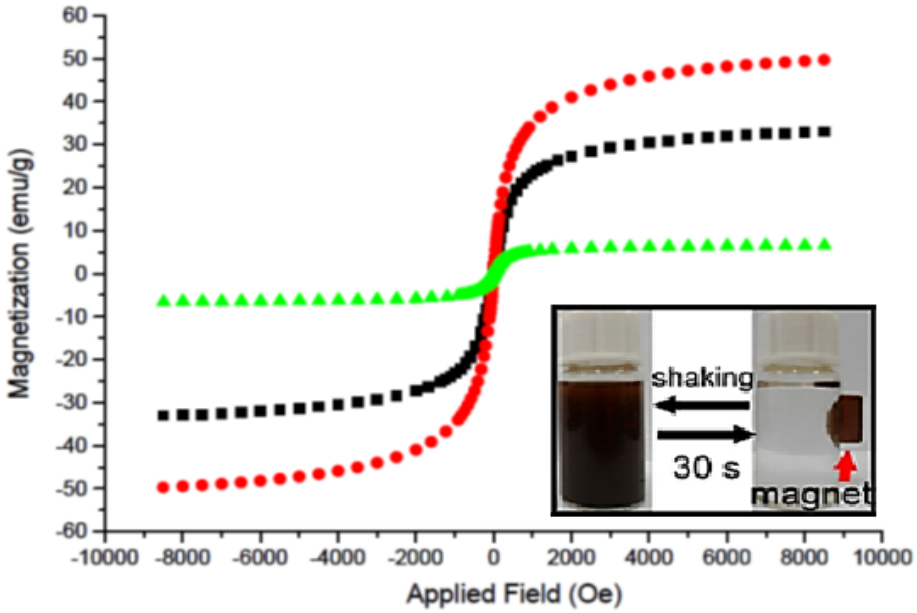

Fig. 6. Magnetization loops of (a) Fe_3O_4, (b) Fe_3O_4@NCs, and (c) Nano Fe_3O_4@cellulose/Ti(IV).

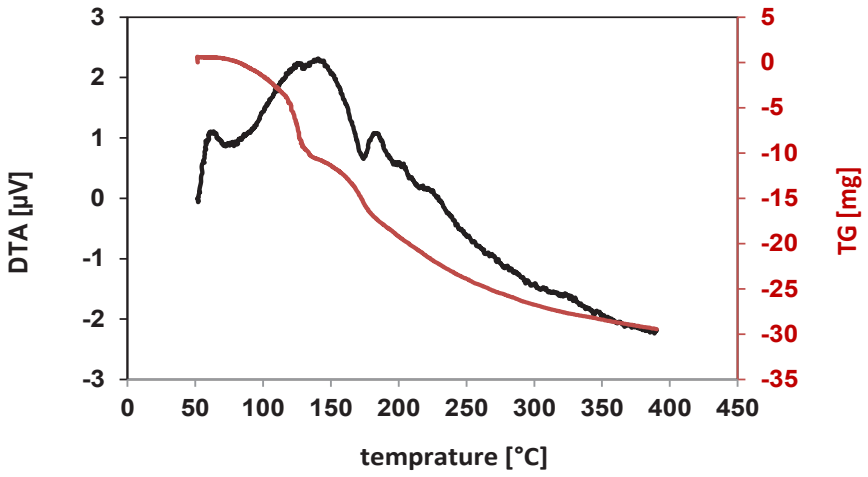

Fig. 7. Thermal gravimetric analysis pattern of Nano Fe_3O_4@cellulose/Ti(IV).

The catalytic activity of nano Fe_3O_4@cellulose/Ti(IV) was investigated for the synthesis of highly functionalized tetrahydropyridines via a five-component condensation reaction of p-substituted anilines, aldehydes and ethyl acetoacetate.

In order to optimize the reaction conditions,

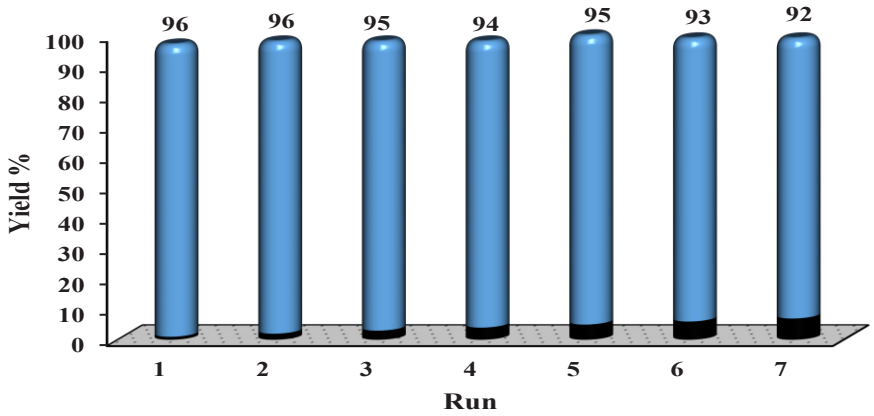

Fig. 8. Recycling experiment.

Table 2. The reaction of 4-ethylaniline, 4-chlorobenzaldehyde, and ethyl acetoacetate in the presence of Nano Fe_3O_4@cellulose/Ti(IV) under various conditions [a].

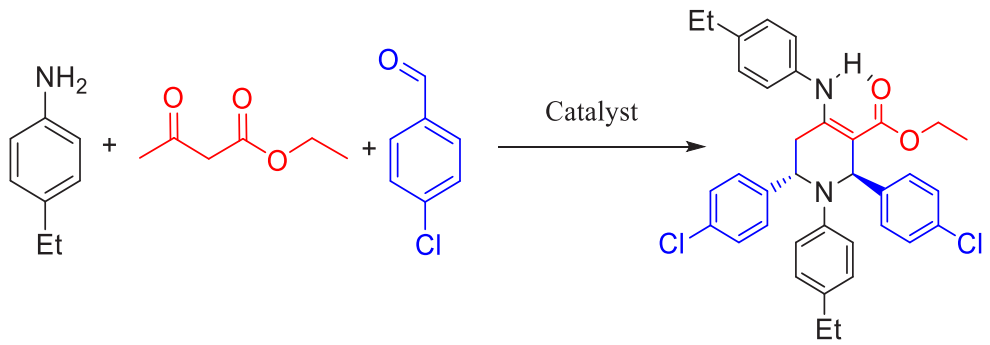

Entry	Solvent	Catalyst (g)	Condition	Time (h)	Yield (%)[b]
1	-	-	80 °C	7	-
2	-	[c] catalyst (0.05)	R. T.	4	15
3	-	[c] catalyst (0.05)	80 °C	3	50
4	C_2H_5OH	[c] catalyst (0.05)	R. T.	4	40
5	C_2H_5OH	[c] catalyst (0.05)	Reflux	3	86
6	CH_3OH	[c] catalyst (0.05)	Reflux	3	41
7	CH_3CN	[c] catalyst (0.05)	Reflux	3	33
8	THF	[c] catalyst (0.05)	Reflux	3	17
9	H_2O	[c] catalyst (0.05)	Reflux	3	22
10	$CHCl_3$	[c] catalyst (0.05)	Reflux	3	3
11	C_2H_5OH	[c] catalyst (0.04)	Reflux	3	82
12	C_2H_5OH	[c] catalyst (0.03)	Reflux	3	92
13	C_2H_5OH	[c] catalyst (0.02)	Reflux	3	70

[a] The amount ratio of 4-ethylaniline (mmol), 4-chlorobenzaldehyde (mmol), and ethyl acetoacetate (mmol) are equal to 2:2:1. [b] Isolated yield. [c] nano Fe_3O_4@cellulose/Ti(IV).

including solvent, temperature, and catalyst loading, the model reaction of 4-ethylaniline, 4-chlorobenzaldehyde, and ethyl acetoacetate was initially carried out under different conditions in the presence of a catalytic amount of nano Fe_3O_4@cellulose/Ti(IV). The results have been

Table 3. Comparative study of the present method and some other reported methods for synthesis of highly functionalized tetrahydropyridines.

Entry	Catalyst	Condition	Time (h)	Yield (%)[a] (Ref)
1[b]	$ZrCl_4$ (15 mol%))	EtOH/ R.T.	16	86 (Aeluri et al. 2012)
2[b]	$Fe(NO_3)_3.9H_2O$ (20 mol%)	EtOH/ R.T.	7	88 (Hazeri et al. 2013)
3[b]	$FeCl_3/SiO_2$ NPs (0.8 mol%)	MeOH/ Reflux	7	86 (Safaei-Ghomi and Ziarati 2013)
4[b]	HOAc (5 ml)	HOAc/ R.T.	7	85 (Lashkari et al. 2013)
5[c]	PTSA.H_2O (0.11 g)	Ethanol/ R.T.	12	88 (Sajadikhah et al. 2012)
6[c]	CAN (15 mol %)	CH_3CN/ R.T.	35	68 (Wang, Mo and Zhang 2011)
7[c]	L-Proline/THF (20 mol %)	CH_3CN/30 °C	22	75 (Misra et al. 2009)
8[d]	Nano Fe_3O_4@cellulose/Ti(IV) (0.03 g)	EtOH/Reflux	3	92 (this work)

[a] Isolated yield. [b] Benzaldehyde, 4-methylaniline and ethyl acetoacetate were used. [c] Benzaldehyde, 4-chloroaniline, and ethyl acetoacetate were used. [d] 4-Chlorobenzaldehyde, 4-ethylaniline, and ethyl acetoacetate were used.

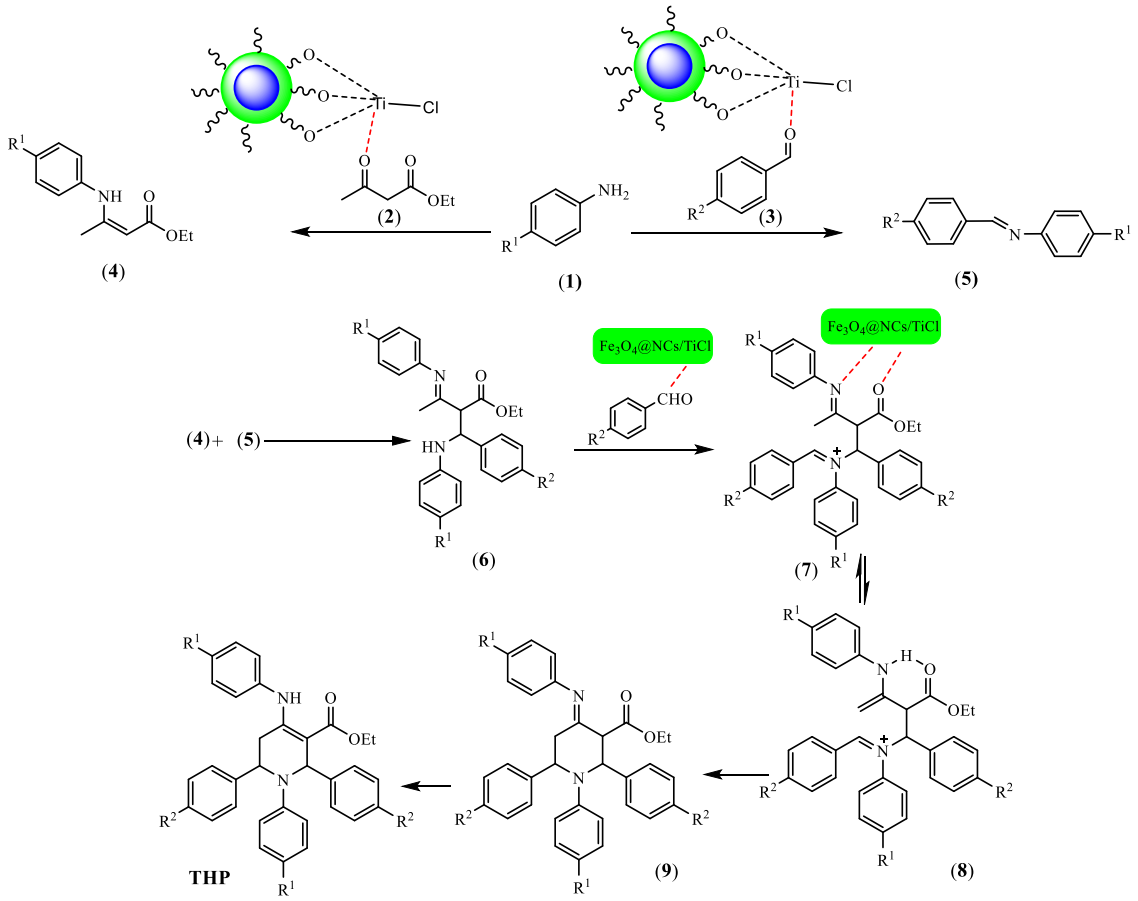

Fig. 9. Proposed mechanism for the multi-component synthesis of THPs IV_{a-n}.

summarized in Table 2. Different solvents including THF, H_2O, CH_3CN, EtOH, MeOH, and $CHCl_3$ were screened (Table 2, Entries 4-10); the model reaction was easier and gave the highest yield in EtOH as solvent under reflux condition (Table 2, Entry 5). To optimize the catalyst amount, the model reaction was performed in the presence of various amounts of the catalyst and according to the obtained results (Table 2, Entries 11-13), 0.03 g of the catalyst was chosen as the best catalyst amount (Table 2, Entry 15). In conclusion, the best reaction condition for this transformation is the use of 0.03 g of the catalyst in EtOH as solvent under reflux condition (Table 2, Entry 12).

The reusability of the catalyst was also investigated in the model reaction. The magnetic nature of the catalyst allowed its facile separation by magnetic decantation, washing with ethanol and drying at room temperature to provide an opportunity for recycling experiments. The separated nano-catalyst was reused in the mentioned reaction seven times without considerable loss of its catalytic activity (Fig. 8). Partial loss of activity may be due to blockage of some active sites of the catalyst and/or partial leaching of titanium from the catalyst.

Comparison of the results of the nano Fe_3O_4@cellulose/Ti(IV)-catalyzed reaction of para-substituted aniline (2 mmol), para-substituted benzaldehyde (2 mmol), and ethyl acetoacetate (1 mmol) with previously reported methods shows the merit of the present protocol (Table 3).

Based on the optimized reaction conditions, a range of THP derivatives were synthesized by the reaction of various *para*-substituted anilines (2 mmol), *para*-substituted benzaldehydes (2 mmol) and ethyl acetoacetate (1 mmol) (Table 4). All compounds were identified by physical and spectroscopic data (mp, FT-IR, and ^{1}H NMR). Moreover, the new products were specified

Table 4. Synthesis of highly functionalized tetrahydropyridines (IV_{a-n}) in the presence of Nano Fe_3O_4@cellulose/Ti(IV) under reflux condition in EtOH [a].

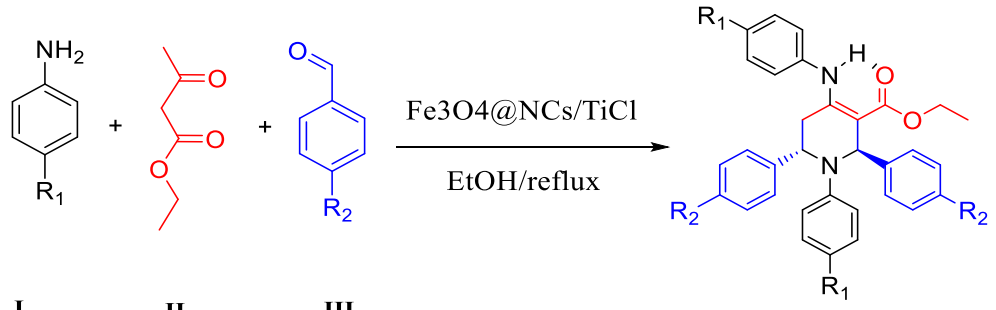

I II III IV

Entry	R^1	R^2	Product	Time (h)	Yield (%)[b]	M.P. (Ref)
1	H	Br	IV_a	1	86	218-220 (Mukhopadhyay et al. 2011)
2	Me	H	IV_b	1	90	193-194 (Hazeri et al. 2013)
3	Me	Br	IV_c	2	89	215-217 -
4	Et	Cl	IV_d	3	92	209-211 -
5	Cl	H	IV_e	1	93	202-204 (Sajadikhah et al. 2012)
6	Cl	Cl	IV_f	2	92	214-215 (Safaei-Ghomi and Ziarati 2013)
7	Br	Cl	IV_g	3	89	193-195 (Mukhopadhyay et al. 2011)
8	Br	OMe	IV_h	1	92	217-219 (Harichandran, Amalraj and Shanmugam 2013)
9	H	Me	IV_i	2	82	228-230 (Harichandran, Amalraj and Shanmugam 2013)
10	H	Cl	IV_j	2	80	202-204 (Mukhopadhyay et al. 2011)
11	Me	Me	IV_k	2	92	170-172 (Hazeri et al. 2013)
12	Et	H	IV_l	1	86	187-189 -
13	Et	Me	IV_m	2	91	176-178 -
14	Br	H	IV_n	1	90	200-202 (Hazeri et al. 2013)

[a] I (mmol):II (mmol):III (mmol):Nano Fe_3O_4@cellulose/Ti(IV) (g) is equal to 2:1:2:0.03. [b] Isolated yield.

using the aforementioned methods as well as ^{13}C NMR spectroscopy and CHN analysis. In the FTIR spectra, the ester C=O stretching frequency appeared around 1650 cm^{-1} due to conjugation

Table 5. The electronic band gap (Eg=EHOMO-ELUMO) and total energy calculations for highly functionalied tetrahydropyridines (IVa-n).

Entry	R^1	R^2	Product	E_{tot} (a.u)	$E_g=E_{HOMO}-E_{LUMO}$
1	H	Br	IV_a	-1720.69144	0.0770
2	Me	H	IV_b	-3400.85873	0.0823
3	Me	Br	IV_c	-3400.65987	0.0820
4	Et	Cl	IV_d	-6606.69325	0.0834
5	Cl	H	IV_e	-7523.27167	0.0868
6	Cl	Cl	IV_f	-6608.48436	0.0839
7	Br	Cl	IV_g	-3564.27990	0.0824
8	Br	OMe	IV_h	-6836.27649	0.0841
9	H	Me	IV_i	-1640.48787	0.0815
10	H	Cl	IV_j	-1564.27932	0.0811
11	Me	Me	IV_k	-6608.48399	0.0830
12	Et	H	IV_l	-1642.48290	0.0819
13	Et	Me	IV_m	-3557.27175	0.0825
14	Br	H	IV_n	-3315.64601	0.0820

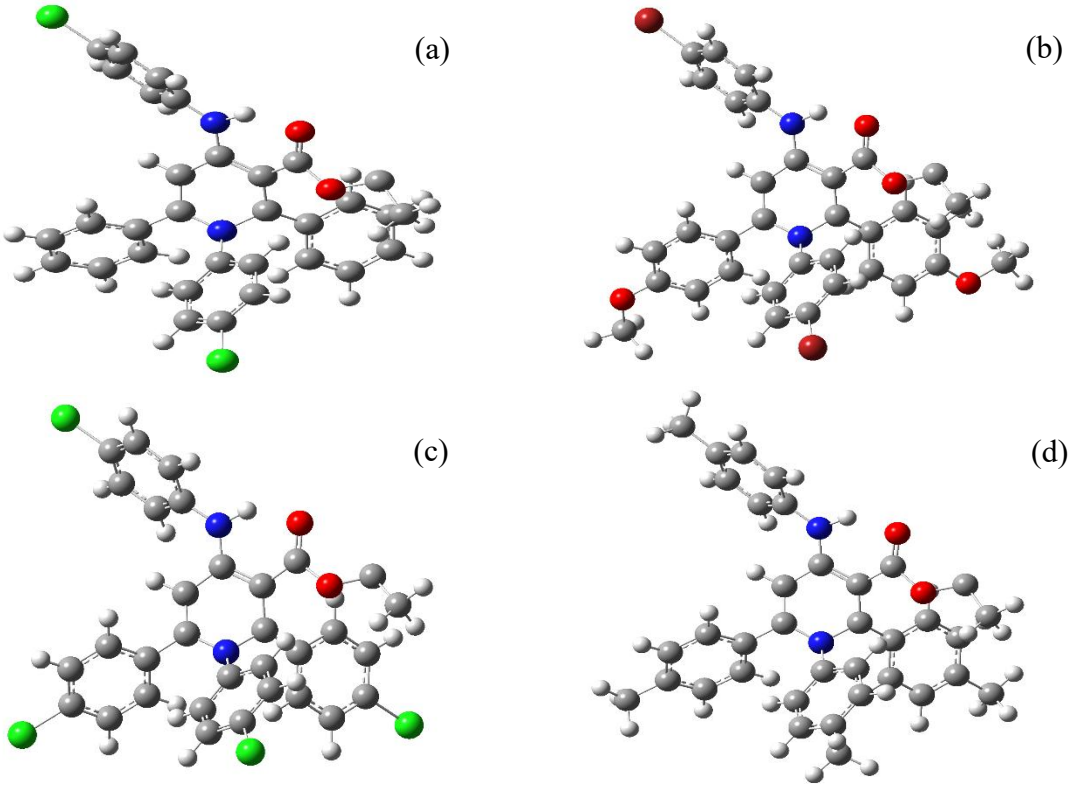

Fig. 10. The relaxed structures for functionalized tetrahydropyridines (a) IVe, (b) IVh, (c) IVf, and (d) IVk.

and hydrogen bonding with N-H. In the ^1H NMR spectra, the distinct peak near δ=10.5 ppm is assigned to N-H of secondary amine-containing hydrogen bonding with the ester C=O group.

A suggestion mechanism for this multi-component reaction was shown in Fig. 9. Titanium in Fe_3O_4@NCs/TiCl activates the C=O group in β-ketoester and aldehyde to promote the β-enaminone (4) or imine (5) formation. The intermolecular Mannich addition of the β-enaminone (4) to the imine (5) affords the intermediate (6). Subsequently, the reaction of activated aldehyde with the intermediate (6) proceeds to afford the intermediate (7) by the elimination of H_2O. Then, tautomerization of (7) generates intermediate (8), which immediately undergoes an intramolecular Mannich-type reaction to give intermediate (9). Finally, the intermediate (9) tautomerizes to generate the desired THP derivative containing a conjugated ester group which bonds to NH with hydrogen bonding.

COMPUTATIONAL DETAILS

Becke's 3-parameter hybrid (B3) exchange functional and the Lee–Yang–Parr correlation functional with 6–311G (d, p) basis sets [58-67] were used to determine the most stable compounds of functionalized tetrahydropyridines (IV_{a-n}). All computations were carried out using Density Functional Theory (DFT) [68-71] as implemented in the Gaussian 09 package [72-77]. The total energy and band gap ($E_g=E_{HOMO}-E_{LUMO}$) calculations for highly functionalized tetrahydropyridines (IV_{a-n}) are given in Table 5. The stability of IV_e compound is higher than that of the other reported compounds, according to total energy and stability statistics.

Additionally, the relaxed structures of functionalized tetrahydropyridines IV_e, IV_h, IV_f and IV_k with the total energy of -7523.27167, -6836.27649, -6608.48436, and -6608.48399 a.u, respectively, are displayed in Fig. 10.

The obtained results illustrated that the functionalized tetrahydropyridines IV_e is more stable than that of the other reported compounds, which is in good agreement with the experimentally reported data.

CONCLUSION

In summary, to make a good contribution to the innovation of green chemistry, we have demonstrated the preparation and characterization of nano Fe_3O_4@cellulose/Ti(IV) as a highly efficient, magnetically recyclable, cheap and novel bio-based heterogeneous catalyst. The catalytic activity of the prepared catalyst was investigated in the synthesis of highly functionalized tetrahydropyridines through one-pot five-component condensation reaction of p-substituted anilines, aldehydes, and ethyl acetoacetate under reflux conditions in EtOH. This procedure offers the advantages of mild reaction conditions, easy work-up, excellent yields, simple magnetic separation of the catalyst, and its recyclability for up to seven cycles without any considerable loss of efficiency. The computation outcomes revealed that the DFT calculation results validated the experimentally reported data.

ACKNOWLEDGEMENTS

The Research Council of Yazd University gratefully acknowledged for the financial support for this work.

CONFLICT OF INTEREST

The authors declare that there is no conflict of interests regarding the publication of this manuscript.

REFERENCES

1. Zheng X, Luo S, Zhang L, Cheng JP, Magnetic nanoparticle supported ionic liquid catalysts for CO_2 cycloaddition reactions. Green Chemistry, (2009); 11(4): 455-458.
2. Jiang Y, Guo C, Xia H, Mahmood I, Liu C, Liu H, Magnetic nanoparticles supported ionic liquids for lipase immobilization: Enzyme activity in catalyzing esterification. Journal of Molecular Catalysis B: Enzymatic, (2009); 58(1): 103-109.
3. Azgomi N, Mokhtary M, Nano-Fe_3O_4@SiO_2 supported ionic liquid as an efficient catalyst for the synthesis of 1, 3-thiazolidin-4-ones under solvent-free conditions. Journal of Molecular Catalysis A: Chemical, (2015); 398: 58-64.
4. Datta A, Adhikary J, Chatterjee S, Ghosh D, Khamarui S, Chattopadhyay T, Synthesis and characterization of a magnetically separable novel Fe_3O_4@L-DOPA@CuII nanocatalyst (L-DOPA=L-3,4-dihydroxyphenyylalanine): Asymmetric aza-Michael addition reaction. Inorganica Chimica Acta, (2016); 444: 209-216.
5. Mukherjee S; Kundu A;, Pramanik A, A new and efficient synthesis of pyrazole-fused isocoumarins on the solid surface of magnetically separable Fe_3O_4@SiO_2-SO_3H nano particles. Tetrahedron Letters, (2016): 57(19), 2103-2108.
6. Yao Y, Miao S, Yu S, Ma LP, Sun H, Wang S, Fabrication of Fe_3O_4/SiO_2 core/shell nanoparticles attached to graphene oxide and its use as an adsorbent. Journal of colloid and interface science, (2012); 379(1): 20-26.
7. Utkan GG, Sayar F, Batat P, Ide S, Kriechbaum M, Pişkin E, Synthesis and characterization of nanomagnetite particles

and their polymer coated forms. Journal of colloid and interface science, (2011); 353(2): 372-379.
8. Mizutani N, Iwasaki T, Watano S, Yanagida T, Tanaka H, Kawai T, Effect of ferrous/ferric ions molar ratio on reaction mechanism for hydrothermal synthesis of magnetite nanoparticles. Bulletin of Materials Science, (2008); 31:713-717.
9. Yang HH, Zhang SQ, Chen XL, Zhuang ZX, Xu JG, Wang XR, Magnetite-containing spherical silica nanoparticles for biocatalysis and bioseparations. Analytical chemistry, (2004); 76(5): 1316-1321.
10. Lu Y, Lu X, Mayers BT, Herricks T, Xia Y, Synthesis and characterization of magnetic Co nanoparticles: A comparison study of three different capping surfactants. Journal of Solid State Chemistry, (2008); 181(7):1530-1538.
11. El Harrak A, Carrot G, Oberdisse J, Eychenne-Baron C, Boue F, Surface−atom transfer radical polymerization from silica nanoparticles with controlled colloidal stability. Macromolecules, (2004); 37(17):6376-6384.
12. Rase HF, Handbook of commercial catalysts: heterogeneous catalysts. CRC Press, New York (2000).
13. Tartaj P, Serna CJ, Synthesis of monodisperse superparamagnetic Fe/silica nano spherical composites. Journal of the American Chemical Society, (2003);125(51):15754-15755.
14. Zhang Z, Duan H, Li S, Lin Y, Assembly of magnetic nanospheres into one-dimensional nanostructured carbon hybrid materials. Langmuir, (2010); 26(9): 6676-6680.
15. Lu AH, Salabas EL, Schuth F, Magnetic nanoparticles: Synthesis, protection, functionalization, and application. Angewandte chemie international edition, (2007); 46(8): 1222-1244.
16. Antonella C, Gabriella DC, Gabriel MI, Cristina R, Daniela Zane, Chiara B, Chitosan stabilized gold nanoparticle-modified au electrodes for the determination of polyphenol index in wines: A preliminary study. Electroanalysis, (2012); 24(4): 897-904.
17. Feng G, Hu D, Yang L, Cui Y, Cui XA, Li H, Immobilized-metal affinity chromatography adsorbent with paramagnetism and its application in purification of histidine-tagged proteins. Separation and purification technology, (2010); 74(2):253-260.
18. Primo A, Quignard F, Chitosan as efficient porous support for dispersion of highly active gold nanoparticles: Design of hybrid catalyst for carbon–carbon bond formation. Chemical communications, (2010); 46(30):5593-5595.
19. Di Carlo G, Curulli A, Toro RG, Bianchini C, De Caro T, Padeletti G, Zane D, Ingo GM, Green synthesis of gold–chitosan nanocomposites for caffeic acid sensing. Langmuir, (2012); 28(12):5471-5479.
20. Brown RMJ, Saxena IM, Cellulose: Molecular and structural biology: Selected articles on the synthesis, structure, and applications of cellulose. Springer Netherlands (2007).
21. Kadla J, Gilbert RD, Cellulose structure: A review. Cellulose Chemistry and Technology, (2000); 34:197-216.
22. Bhattacharya SS, Shukla S, Banerjee S, Chowdhury P, Chakraborty P, Ghosh A, Tailored IPN hydrogel bead of sodium carboxymethyl cellulose and sodium carboxymethyl xanthan gum for controlled delivery of diclofenac sodium. Polymer-Plastics Technology and Engineering, (2013); 52(8): 795-805.
23. Czaja WK, Young DJ, Kawecki M, Brown RM, The future prospects of microbial cellulose in biomedical applications. biomacromolecules, (2007); 8(1):1-12.
24. Patchan M, Graham J, Xia Z, Maranchi J, McCally R, Schein O, Elisseeff J, Trexler M, Synthesis and properties of regenerated cellulose-based hydrogels with high strength and transparency for potential use as an ocular bandage. Materials Science and Engineering: C, (2013); 33(5):3069-3076.
25. Sannino A, Esposito A, Nicolais L, Del Nobile MA, Giovane A, Balestrieri C, Esposito R, Agresti M, Cellulose-based hydrogels as body water retainers. Journal of materials science: materials in medicine, (2000); 11:247-253.
26. Sarvas M, Pavlenda P, Takacova E, Effect of hydrogel application on survival and growth of pine seedlings in reclamations. Journal of forest science, (2007); 53(5): 204-209.
27. Sklenar Z, Vitkova Z, Herdova P, Horackova K, Simunkova V, Formulation and release of alaptide from cellulose-based hydrogels. Acta Veterinaria Brno, (2013); 81(3): 301-306.
28. Chavan PV, Pandit KS, Desai UV, Kulkarni MA, Wadgaonkar PP, Cellulose supported cuprous iodide nanoparticles (Cell-CuI NPs): A new heterogeneous and recyclable catalyst for the one pot synthesis of 1, 4-disubstituted–1, 2, 3-triazoles in water. RSC advances, (2014); 4 (79): 42137-42146.
29. Shaabani A, Maleki A, Cellulose sulfuric acid as a bio-supported and recyclable solid acid catalyst for the one-pot three-component synthesis of α-amino nitriles. Applied Catalysis A: General, (2007); 331:149-151.
30. Domino KB, Anderson EA, Polissar NL, Posner KL, Comparative efficacy and safety of ondansetron, droperidol, and metoclopramide for preventing postoperative nausea and vomiting: A meta-analysis. Anesthesia & Analgesia, (1999); 88(6):1370-1379.
31. Mashkovskii M, Glushkov R, Drugs for the treatment of alzheimer's disease. Pharmaceutical Chemistry Journal, (2001); 35(4):179-182.
32. Aeluri R, Alla M, Bommena VR, Murthy R, Jain N, Synthesis and antiproliferative activity of polysubstituted tetrahydropyridine and piperidin4-one-3-carboxylate derivatives. Asian Journal of Organic Chemistry, (2012); 1(1): 71-79.
33. Misra M, Pandey SK, Pandey VP, Pandey J, Tripathi R, Tripathi RP, Organocatalyzed highly atom economic one pot synthesis of tetrahydropyridines as antimalarials. Bioorganic & Medicinal Chemistry, (2009);17(2):625-633.
34. Kitagawa H, Takenouchi T, Azuma R, Wesnes KA, Kramer WG, Clody DE, Burnett AL, Safety, pharmacokinetics, and effects on cognitive function of multiple doses of GTS-21 in healthy, male volunteers. Neuropsychopharmacology, (2003); 28(3): 542-551.
35. Newman-Tancredi A, Heusler P, Martel JC, Ormiere AM, Leduc N, Cussac D, Agonist and antagonist properties of antipsychotics at human dopamine D4.4 receptors: G^- protein activation and K^+ channel modulation in transfected cells. International Journal of Neuropsychopharmacology, (2008); 11(3): 293-307.
36. Powell SB, Paulus MP, Hartman DS, Godel T, Geyer MA, RO-10-5824 is a selective dopamine D4 receptor agonist that increases novel object exploration in C57 mice. Neuropharmacology, (2003); 44(4): 473-481.
37. Clarke PA, Zaytzev AV, Whitwood AC, Pot, atom and step economic (PASE) synthesis of highly functionalized piperidines: A five-component condensation. Tetrahedron Letters, (2007); 48(30): 5209-5212.

38. Clarke PA, Zaytsev AV, Whitwood AC, Pot, atom, and step economic (PASE) synthesis of highly substituted piperidines: A five-component condensation. Synthesis, (2008); 21: 3530-3532.
39. Khan AT, Parvin T, Choudhury LH, Effects of substituents in the β-Position of 1,3-dicarbonyl compounds in bromodimethylsulfonium bromide-catalyzed multicomponent reactions: A facile access to functionalized piperidines. The Journal of Organic Chemistry, (2008); 73 (21): 8398-8402.
40. Khan AT, Lal M, Khan MM, Synthesis of highly functionalized piperidines by one-pot multicomponent reaction using tetrabutylammonium tribromide (TBATB). Tetrahedron Letters, (2010); 51(33): 4419-4424.
41. Khan AT, Khan MM, Bannuru KKR, Iodine catalyzed one-pot five-component reactions for direct synthesis of densely functionalized piperidines. Tetrahedron, (2010); 66(39): 7762-7772.
42. Wang HJ, Mo LP, Zhang ZH, Cerium ammonium nitrate-catalyzed multicomponent reaction for efficient synthesis of functionalized tetrahydropyridines. ACS Combinatorial Science, (2011); 13(2):181-185.
43. Mishra S, Ghosh R, Efficient one-pot synthesis of functionalized piperidine scaffolds via $ZrOCl_2{\cdot}8H_2O$ catalyzed tandem reactions of aromatic aldehydes with amines and acetoacetic esters. Tetrahedron Letters, (2011); 52(22):2857-2861.
44. Sajadikhah SS, Maghsoodlou MT, Hazeri N, Habibi-Khorassani SM, Shams-Najafi SJ, One-pot multicomponent synthesis of highly substituted piperidines using p-toluene sulfonic acid monohydrate as catalyst. Monatshefte fur Chemie-Chemical Monthly, (2012); 143(6): 939-945.
45. Hazeri N, Maghsoodlou MT, Habibi-Khorassani SM, Aboonajmi J, Sajadikhah SS, $Fe(NO_3)_3{\cdot}9H_2O$ as efficient catalyst for one-pot synthesis of highly functionalized piperidines. Journal of the Chinese Chemical Society, (2013); 60(4):355-358.
46. Safaei-Ghomi J, Ziarati A, An efficient $FeCl_3/SiO_2$ NPs as a reusable heterogeneous catalyzed five-component reactions of tetrahydropyridines under mild conditions. Journal of the Iranian Chemical Society, (2013); 10(1):135-139.
47. Harichandran G, Amalraj SD, Shanmugam P, A facile and efficient solid supported, one-pot synthesis of functionalized piperidine derivatives catalyzed by amberlite IRA400-Cl Resin/I2/KI via Multicomponent reaction. Journal of Heterocyclic Chemistry, (2013); 50(3): 539-543.
48. Lashkari M, Maghsoodlou MT, Hazeri N, Habibi-Khorassani SM, Sajadikhah SS, Doostmohamadi R, Synthesis of highly functionalized piperidines via one-pot, five-component reactions in the presence of acetic acid solvent. Synthetic Communications, (2013); 43(5): 635-644.
49. Ramachandran R, Jayanthi S, Jeong YT, One-pot synthesis of highly diversified tetrahydropyridines by tandem condensation of aldehydes, amines, and β-ketoesters. Tetrahedron, (2012); 68(1):363-369.
50. Daraei M, Zolfigol MA, Derakhshan-Panah F, Shiri M, Kruger HG, Mokhlesi M, Synthesis of tetrahydropyridines by one-pot multicomponent reaction using nano-sphere silica sulfuric acid. Journal of the Iranian Chemical Society, (2015); 12(5):855-861.
51. Eshghi H, Khojastehnezhad A, Moeinpour F, Bakavoli M, Seyedi SM, Abbasi M, Synthesis, characterization and first application of keggin-type heteropoly acids supported on silica coated $NiFe_2O_4$ as novel magnetically catalysts for the synthesis of tetrahydropyridines. RSC Advances, (2014); 4(75):39782-39789.
52. Valbe R, Tarkanovskaja M, Maeorg U, Reedo V, Hoop A, Kink I, Lohmus A, Elaboration of hybrid cotton fibers treated with an ionogel/carbon nanotube mixture using a sol-gel approach. Open Chemistry, (2015); 13(1):279-286.
53. Zhu Y, Zhang L, Gao C, Cao L, The synthesis of nanosized TiO_2 powder using a sol-gel method with $TiCl_4$ as a precursor. Journal of Materials Science, (2000); 35(16):4049-4054.
54. Ryu HK, Heo JS, Cho SI, Moon SH, Thermal decomposition mechanism of $Ti(OiPr)_2$ $(DPM)_2$. Journal of The Electrochemical Society, (1999); 146(3):1117-1121.
55. Keller OL Jr, Identification of complex ions of Niobium (V) in hydrofluoric acid solutions by raman and infrared spectroscopy. Inorganic Chemistry, (1963); 2(4):783-787.
56. Jang JH, Lim HB, Characterization and analytical application of surface modified magnetic nanoparticles. Microchemical Journal, (2010); 94(2):148-158.
57. Rosli N, Ahmad I, Abdullah I, Isolation and characterization of cellulose nanocrystals from agave angustifolia fibre. BioResources, (2013); 8(2):1893-1908.
58. Becke AD, Density-functional exchange-energy approximation with correct asymptotic behavior. Physical Review A, (1988); 38(6):3098-3100.
59. Lee C, Yang W, Parr RG, Development of the Colle-Salvetti correlation-energy formula into a functional of the electron density. Physical Review B, (1988); 37(2):785-789.
60. Hou X, Ren Y, Fu F, A density functional theory study on the electronic and adsorption characteristics of cyclo M_9N_9 (M=B and Al). Journal of Molecular Modeling, (2020); 26(10): 1-10.
61. Dolatabad AA, Salehpour M, Saadati Z, Hexa-peri-hexabenzocoronene as a vector sensing and delivery of carmustine anticancer drug: A density functional theory study. Journal of Molecular Liquids, (2024); 407:125206.
62. Zaharim WN, Sulaiman S, Jamaludin A, Rozak H, Watanabe I, Density functional theory investigation of electronic structure and muon hyperfine interaction in isolated adenine and thymine. Interactions, (2024); 245: 47.
63. Deraet X, Cilesiz U, Aviyente V, De Proft F, Structural and energetic properties of cluster models of anatase-supported single late transition metal atoms: A density functional theory benchmark study. Journal of Molecular Modeling. (2024); 30:1-13.
64. Watts HD, Kubicki JD, Pedentchouk N, Freeman KH, Position-Specific 2H/H equilibrium isotopic fractionation factors in alkane, alkene, and aromatic molecules: A density functional theory approach. ACS Earth and Space Chemistry, (2024); 8: 21-35.
65. Asemare S, Belay A, Kebede A, Sherfedin U, Ground and excited state dipole moments of metformin hydrochloride using solvatochromic effects and density functional theory. Journal of Fluorescence, (2024), 34:1207-1217.
66. Mishra M, DFT study of difluoro & trifluoro bi-cyclohexane based dimer for application in electronic and optical devices. Journal of Molecular Liquids, (2024); 414:126109.
67. Yao J, Li DS, Qiu J, Xu X, Yang HY, How boron is adsorbed by oxygen-containing groups functionalized graphene: A density functional theory study. Sep Purif Technol, (2024); 330: 125551.
68. Kohn W, Sham LJ, Self-Consistent equations including

exchange and correlation effects. Physical Review, (1965); 140(4A):1133-1138.
69. Malik Y, Unveiling the unique properties of carbon nitride (C_6N_8) monolayer as a novel flexible sensor for hydrogen cyanide and hydrogen fluoride: A DFT study. Diamond and Related Materials, (2024); 143:110930.
70. Gul M, Synthesis and evaluation of some novel 1, 3-Dimethylbarbituric Acid derivatives as potent anti-urease agents: Comprehension through in vitro, molecular docking, and DFT investigations. Russian Journal of Bioorganic Chemistry, (2024); 50:1609-1626.
71. Boucherdoud A, Experimental exploration and DFT analysis of the kinetics and mechanism of malachite green photodegradation catalyzed by polyaniline-copper oxide nanocomposite. Journal of Molecular Modeling, (2024); 30:235.
72. Frisch MJ, Trucks G, Schlegel HB, Scuseria GE, Robb MA, Cheeseman J, Scalmani G, Barone V, Mennucci B, Petersson GA, Nakatsuji H, Caricato M, Li X, Hratchian HP, Izmaylov AF, Bloino J, Zheng G, Sonnenberg J, Hada M, Fox D, Gaussian 09 Revision A.1. Gaussian Inc. (2009).
73. Aljeboree AM, Radia ND, Jasim LS, Alwarthan AA, Khadhim MM, Washeel Salman A, Alkaim AF, Synthesis of a new nanocomposite with the core TiO_2/hydrogel: Brilliant green dye adsorption, isotherms, kinetics, and DFT studies. Journal of Industrial and Engineering Chemistry, (2022); 109:475-485.
74. Taha H, El Mahdy A, Lebda H, Adsorption of gases on doped graphene quantum dots with (TM= Ni, Pd, and Pt): DFT and TD-DFT investigation. Physica B: Condensed Matter, (2024); 676:415667.
75. El-Sayed NM, Elhaes H, Ibrahim A, Ibrahim MA, Investigating the electronic properties of edge glycine/biopolymer/graphene quantum dots. Sci Rep, (2024); 14:21973.
76. Velho P, Oliveira RA, Macedo ENA, Correlating excess volumes for binary mixtures of green solvents with the help of density functional theory. Industrial & Engineering Chemistry Research, (2024); 63:15990-15998.
77. Xiao JL, Synthesis, crystal structure and DFT study of N-(6-sulfamoylpyridin-3-yl) acetamide. Molecular Crystals and Liquid Crystals, (2023); 758: 36-45.